

## Three-dimensional instability of a two-layer Dean flow

Alexander Yu. Gelfgat, Alexander L. Yarin, and Pinhas Z. Bar-Yoseph  
*Computational Mechanics Laboratory, Faculty of Mechanical Engineering,  
Technion-Israel Institute of Technology, Haifa 32000, Israel*

(Received 6 March 2001; accepted 24 July 2001)

Stability of a two-layer Dean flow in a cylindrical annulus with respect to three-dimensional perturbations is studied by a global Galerkin method. It is shown that for large inner radius of the annulus (i) the instability becomes three-dimensional if one of the fluid layers is thin, (ii) its onset is not affected by possible small deformations of the interface, and (iii) multiple three-dimensional flow states are expected in a slightly supercritical flow regime. Stability diagrams and patterns of the three-dimensional perturbations are reported. It is concluded that even when the axisymmetric perturbation is the most dangerous, the resulting supercritical flow is expected to be three-dimensional. Possible multiplicity of supercritical three-dimensional states is predicted. The basis functions of the global Galerkin method are constructed so as to satisfy analytically the boundary conditions on no-slip walls and at the liquid-liquid interface. A modification of the numerical approach, accounting for small deformations of the interface which is subject to the action of the capillary force, is proposed. The results are of potential importance for development of novel bioseparators employing Dean vortices for enhancement of mass transfer of a passive scalar (say, a protein) through the interface. The developed numerical approach can be used for stability analysis in other two-fluid systems. © 2001 American Institute of Physics.  
[DOI: 10.1063/1.1409967]

### I. INTRODUCTION

The classical Dean problem considers the flow of an incompressible Newtonian fluid driven by an azimuthal pressure gradient in a cylindrical annulus. The instability of this flow leads to creation of so-called Dean vortices.<sup>1-3</sup> Stability analysis of this problem explains this effect in Poiseuille-type flows in curved pipes and channels.<sup>4</sup> At present the Dean vortices are known as a means for intensification of heat<sup>5</sup> and mass<sup>6</sup> transfer in single-phase liquids. Recently, certain attempts were made to intensify mass transfer of a passive scalar through a boundary separating two immiscible liquids by creating spatially periodic vortical flows inside both liquid phases, using a two-fluid Taylor-Couette apparatus.<sup>7,8</sup> Obviously, Dean flow is another possible originator of vortical flow inside a two-fluid system, and a potential candidate as a new element in novel bioseparators for protein extraction.

In the present work we study the onset of Dean vortices in the two-fluid Dean problem (Fig. 1). Namely, stability of a flow driven by a constant azimuthal pressure gradient in a cylindrical annulus filled with two immiscible liquid layers is considered. The liquid-liquid interface can be (i) nondeformable or (ii) deformable and subject to capillary forces. In the latter case small perturbations of the interface are included in the formulation of the stability problem. The gravity effect is disregarded.

The stability problem is solved using an extension of the global Galerkin approach<sup>9,10</sup> for stability analysis of viscous single-phase flows in confined domains. This approach uses linear superpositions of Chebyshev polynomials to satisfy analytically no-slip or stress-free boundary conditions. In the

present work we describe how the Galerkin basis can be constructed for a two-fluid case such that not only no-slip conditions, but also those of continuity and the balance of viscous stresses at the liquid-liquid interface are satisfied analytically. Then we show how the balance of the capillary and normal viscous stresses can be included in the numerical model assuming small deformations of the interface. The proposed approach can be used for stability analysis of various two-fluid systems,<sup>10,11</sup> e.g., for two-layer Rayleigh-Bénard<sup>12</sup> or Taylor-Couette<sup>13</sup> flows.

The stability analysis in the present work, which accounts for three-dimensional perturbations and for possible small deformations of the liquid-liquid interface, leads to two main conclusions. First, the instability observed in the system corresponds to onset of vortical motion and is not affected by deformations of the interface. Second, the instability is axisymmetric when the depths of both layers do not differ significantly, i.e., the value of  $b/d$  is close to 0.5. When one of the layers is thin (i.e.,  $b$  is close to zero or to the gap thickness  $d$ ), the instability is caused by a nonaxisymmetric three-dimensional perturbation characterized by a relatively high azimuthal wave number. Location of the interface (the value of  $b$ ) corresponding to the switch between the axisymmetric and three-dimensional instabilities depends on other governing parameters. In particular, a strong dependence on the ratio of viscosities of two fluids is found. On the basis of the calculated stability diagrams, we predict existence of multiple three-dimensional supercritical flow states, which appear as spiraling waves that rotate about the axis and propagate along it. Spatial patterns of the nonaxisymmetric perturbations are illustrated.

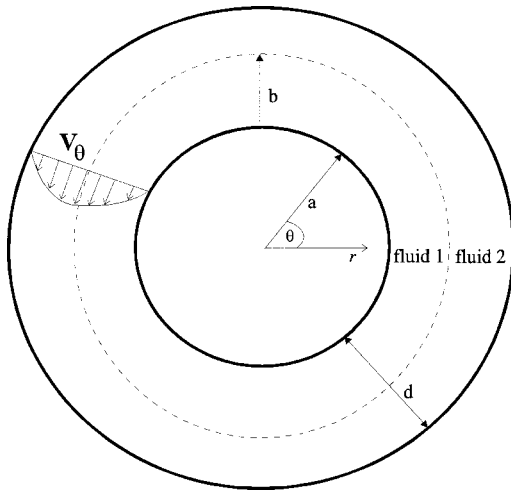


FIG. 1. Sketch of the problem.

The paper is organized as follows. Formulation of the problem is discussed in Sec. II. The basic flow is considered in Sec. III. Stability problems for nondeformable and deformable interfaces are considered in Sec. IV. The numerical method is described in Sec. V. The results are reported in Sec. VI. Conclusions are drawn in Sec. VII.

**II. FORMULATION OF THE PROBLEM**

Consider a cylindrical annulus, whose radius varies in the interval  $a \leq r \leq a + d$ , filled with two immiscible Newtonian incompressible liquids 1 and 2 which, in the unperturbed state, occupy cylindrical layers  $a \leq r \leq a + b$  and  $a + b \leq r \leq a + d$ , respectively (see Fig. 1). It is assumed that the flow is driven by a constant azimuthal pressure gradient  $\partial p / \partial \theta = G = \text{const}$ . The velocity and pressure fields in each liquid satisfy the Navier–Stokes equations:

$$\rho_i \left[ \frac{\partial \mathbf{v}_i}{\partial t} + (\mathbf{v}_i \cdot \nabla) \mathbf{v}_i \right] = - \frac{G}{r} \mathbf{e}_\theta - \nabla P_i + \eta_i \Delta \mathbf{v}_i, \tag{1a}$$

$$\nabla \cdot \mathbf{v}_i = 0, \tag{1b}$$

where  $\mathbf{v}_i = \{U_i, V_i, W_i\}$  is the flow velocity,  $P_i$  the pressure additional to the component responsible for the azimuthal pressure gradient,  $\rho_i$  the density and  $\eta_i$  the dynamic viscosity of liquid  $i$ .  $U_i$ ,  $V_i$ , and  $W_i$  denoting the radial, azimuthal, and axial velocities, respectively, and the subscript  $i$  referring to liquids 1 and 2. The no-slip boundary conditions are imposed at the boundaries of the annulus

$$\text{at } r = a: \quad \mathbf{v}_1 = \mathbf{0}, \tag{2a}$$

$$\text{at } r = a + d: \quad \mathbf{v}_2 = \mathbf{0}. \tag{2b}$$

At the interface we impose the conditions of continuity of the velocity vector and shear stress, as well as a jump of the normal stress due to the surface tension.

For nondimensionalization of the problem we use the velocity scale  $v_0 = (G/\rho_1)^{1/2}$ . As the length, pressure and time scales we use  $d$ ,  $\rho_1 v_0^2$ , and  $d/v_0$ , respectively.

The dimensionless governing equations read

$$\frac{\partial \mathbf{v}_i}{\partial t} + (\mathbf{v}_i \cdot \nabla) \mathbf{v}_i = - \frac{1}{\rho_{1i}} \frac{1}{r} \mathbf{e}_\theta - \frac{1}{\rho_{1i}} \nabla P_i + \frac{\eta_{1i}}{\rho_{1i}} \frac{1}{\text{Re}} \Delta \mathbf{v}_i, \tag{3a}$$

$$\nabla \cdot \mathbf{v}_i = 0, \tag{3b}$$

where  $\text{Re} = \rho_1 d v_0 / \eta_1 = (d/\eta_1) \sqrt{G \rho_1}$  is the Reynolds number, and  $\rho_{1i} = \rho_i / \rho_1$ ,  $\eta_{1i} = \eta_i / \eta_1$ . For convenience of comparison with the previous studies<sup>1–4</sup> we introduce the Dean number  $De = \text{Re} / \sqrt{\bar{a}}$  which accounts also for the radius of curvature of the cylindrical annulus ( $\bar{a} = a/d$ ).

**III. BASIC FLOW**

The velocity of the basic flow is represented by the azimuthal component only, which depends on the radial coordinate, i.e.,  $\mathbf{V} = \{0, V(r), 0\}$  and  $P = p(r)$ . The problem for  $V(r)$  follows from (2) and (3):

$$\frac{1}{r} = \frac{\eta_{1i}}{\text{Re}} \frac{\partial^2 V_i}{\partial r^2}, \tag{4a}$$

$$V_1(\bar{a}) = V_2(\bar{a} + 1) = 0, \tag{4b}$$

$$V_1(\bar{a} + \bar{b}) = V_2(\bar{a} + \bar{b}), \tag{4c}$$

$$\left[ \frac{\partial V_1}{\partial r} \right]_{r=\bar{a}+\bar{b}} = \eta_{1i} \left[ \frac{\partial V_2}{\partial r} \right]_{r=\bar{a}+\bar{b}} \tag{4d}$$

where  $\bar{b} = b/d$ . Following Dean<sup>1</sup> we introduce the new dimensionless coordinate  $x = r - \bar{a}$  and assume that  $\bar{a} \gg 1$  (i.e., the inner radius is large as compared to the gap). This allows one to replace  $r = \bar{a} + x$  by  $\bar{a}$  and reduces (4) to the following form:

$$\frac{1}{\bar{a}} = \frac{\eta_{1i}}{\text{Re}} \frac{\partial^2 V_i}{\partial x^2}, \tag{5a}$$

$$V_1(0) = V_2(1) = 0, \tag{5b}$$

$$V_1(\bar{b}) = V_2(\bar{b}), \tag{5c}$$

$$\left[ \frac{\partial V_1}{\partial x} \right]_{x=\bar{b}} = \eta_{1i} \left[ \frac{\partial V_2}{\partial x} \right]_{x=\bar{b}}. \tag{5d}$$

The solution of (5) reads

$$V_1 = \frac{\text{Re}}{2\bar{a}} x^2 + \frac{\eta_{12}}{\rho_{12}} \frac{\text{Re}}{2\bar{a}} \frac{\bar{b}^2(\rho_{12}/\eta_{12} - 1) - \rho_{12}/\eta_{12}}{\bar{b}(\eta_{12}/\rho_{12} - 1) + 1} x, \tag{6a}$$

$$V_2 = \frac{\rho_{12}}{\eta_{12}} \frac{\text{Re}}{2\bar{a}} x^2 + \frac{\text{Re}}{2\bar{a}} \frac{\bar{b}^2(\rho_{12}/\eta_{12} - 1) - \rho_{12}/\eta_{12}}{\bar{b}(\eta_{12}/\rho_{12} - 1) + 1} x - \frac{\text{Re}}{2\bar{a}} \frac{\bar{b}(1 - \rho_{12}/\eta_{12}) + \bar{b}^2(\rho_{12}/\eta_{12} - 1)}{\bar{b}(\eta_{12}/\rho_{12} - 1) + 1}, \tag{6b}$$

which is an extension of the basic flow of Dean<sup>1</sup> for a two-fluid system.

**IV. STABILITY PROBLEM**

Consider the linear stability problem for the basic state described by (6a) and (6b). Let  $\mathbf{u}=(u,v,w)$  and  $p$  be infinitesimally small perturbations of the velocity and additional pressure, respectively. Using the  $2\pi$ -periodicity in the azimuthal  $\theta$ -direction and assuming a  $2\pi/k$ -periodicity in the axial  $z$  direction, the perturbations can be represented as  $\mathbf{u}_i=(u_i(x),v_i(x),w_i(x))\exp[in\theta+ikz+\lambda t]$ ,  $p_i=p_i(x)\exp[in\theta+ikz+\lambda t]$ , where  $n$  is integer and  $k$  real, both of them dimensionless. Using (3) and (6) we arrive at the following linearized equations:

$$\begin{aligned} \lambda u_i + \frac{in}{\bar{a}+x} V_i u_i - \frac{2}{\bar{a}+x} V_i v_i &= -\frac{1}{\rho_{1i}} \frac{dp_i}{dx} + R_i \left[ \frac{d^2 u_i}{dx^2} + \frac{1}{\bar{a}+x} \frac{du_i}{dx} - \frac{n^2+1}{(\bar{a}+x)^2} u_i \right. \\ &\quad \left. - k^2 u_i - \frac{2in}{(\bar{a}+x)^2} v_i \right], \end{aligned} \tag{7a}$$

$$\begin{aligned} \lambda v_i + u_i \frac{dV_i}{dx} + \frac{in}{\bar{a}+x} V_i v_i + \frac{1}{\bar{a}+x} V_i u_i &= -\frac{in}{\rho_{1i}(\bar{a}+x)} p_i + R_i \left[ \frac{d^2 v_i}{dx^2} + \frac{1}{\bar{a}+x} \frac{dv_i}{dx} \right. \\ &\quad \left. - \frac{n^2+1}{(\bar{a}+x)^2} v_i - k^2 v_i + \frac{2in}{(\bar{a}+x)^2} u_i \right], \end{aligned} \tag{7b}$$

$$\begin{aligned} \lambda w_i + \frac{in}{\bar{a}+x} V_i w_i &= -\frac{ik}{\rho_{1i}} p_i + R_i \left[ \frac{d^2 w_i}{dx^2} + \frac{1}{\bar{a}+x} \frac{dw_i}{dx} - \frac{n^2}{(\bar{a}+x)^2} w_i - k^2 w_i \right], \end{aligned} \tag{7c}$$

$$\frac{du_i}{dx} + \frac{u_i}{\bar{a}+x} + \frac{in}{\bar{a}+x} v_i + ikw_i = 0, \tag{7d}$$

where  $R_i = \eta_{1i}/(\text{Re}\rho_{1i})$ .

Now we recall the assumption  $\bar{a} \gg 1$ . Thus, we replace in (7)  $\bar{a}+x$  by  $\bar{a}$  and drop all terms proportional to  $1/\bar{a}$  and  $1/\bar{a}^2$ . However, assuming that the Reynolds number can be large, we do not drop the terms proportional to  $\text{Re}/\bar{a}$  and therefore retain those proportional to the basic flow  $V$  (those proportional to  $V/\bar{a} \sim \text{Re}/\bar{a}$  were dropped in Ref. 3). Moreover, the basic flow  $V(x)$  has at least one maximum in the interval  $\bar{a} < x < \bar{a}+1$ , where  $dV_i/dx=0$ . Near this point the last two terms on the left-hand side of (7b) are not negligible relative to  $u_i dV_i/dx$ . The simplified governing equations thus read

$$\lambda u_i + \frac{in}{\bar{a}} V_i u_i - \frac{2}{\bar{a}} V_i v_i = -\frac{1}{\rho_{1i}} \frac{dp_i}{dx} + R_i \left[ \frac{d^2 u_i}{dx^2} - k^2 u_i \right], \tag{8a}$$

$$\begin{aligned} \lambda v_i + u_i \frac{dV_i}{dx} + \frac{in}{\bar{a}} V_i v_i + \frac{1}{\bar{a}} V_i u_i &= -\frac{in}{\rho_{1i}\bar{a}} p_i + R_i \left[ \frac{d^2 v_i}{dx^2} - k^2 v_i \right], \end{aligned} \tag{8b}$$

$$\lambda w_i + \frac{in}{\bar{a}} V_i w_i = -\frac{ik}{\rho_{1i}} p_i + R_i \left[ \frac{d^2 w_i}{dx^2} - k^2 w_i \right], \tag{8c}$$

$$\frac{du_i}{dx} + ikw_i = 0. \tag{8d}$$

Solving (8d) for  $w_i$  and (8c) for  $p_i$ , the following eigenvalue problem for  $u_i$  and  $v_i$  is obtained:

$$\lambda D u_i = R_i D^2 u_i - \frac{in}{\bar{a}} V_i D u_i - \frac{in}{\bar{a}} \frac{dV_i}{dx} \frac{du_i}{dx} - \frac{2k^2}{\bar{a}} V_i v_i, \tag{9a}$$

$$\begin{aligned} \lambda \left[ v_i - \frac{in}{\bar{a}k^2} \frac{du_i}{dx} \right] &= R_i D v_i - \frac{dV_i}{dx} u_i - \frac{in}{\bar{a}k^2} \frac{\eta_{1i}}{\rho_{1i}} \frac{1}{\text{Re}} \frac{d}{dx} D u_i \\ &\quad - \frac{n^2 V_i}{\bar{a}^2 k^2} \frac{du_i}{dx} - \frac{in V_i}{\bar{a}} v_i - \frac{V_i}{\bar{a}} u_i, \end{aligned} \tag{9b}$$

where  $D = d^2/dx^2 - k^2$ .

In the case of a nondeformable liquid–liquid interface the necessary boundary conditions for the perturbations take the form (note that  $-ikw_i = du_i/dx$ )

$$\text{at } x=0: \quad u_1 = v_1 = \frac{du_1}{dx} = 0, \tag{10a}$$

$$\text{at } x=1: \quad u_2 = v_2 = \frac{du_2}{dx} = 0, \tag{10b}$$

$$\text{at } x=\bar{b}: \quad u_1 = u_2 = 0, \tag{10c}$$

$$v_1 = v_2, \tag{10d}$$

$$\frac{du_1}{dx} = \frac{du_2}{dx}, \tag{10e}$$

$$\frac{dv_1}{dx} = \eta_{12} \frac{dv_2}{dx}, \tag{10f}$$

$$\frac{d^2 u_1}{dx^2} = \eta_{12} \frac{d^2 u_2}{dx^2}. \tag{10g}$$

It is emphasized that the boundary condition (10e) reflects, in fact, the continuity of the velocity component  $w$ . The boundary conditions (10f) and (10g) express continuity of the shear stresses at the interface.

If the liquid–liquid interface is deformable, the boundary conditions (10c) should be replaced by

$$\text{at } x=\bar{b}: \quad u_1 = u_2 (\neq 0), \tag{11}$$

whereas (10d) and (10e) do not change. An additional boundary condition needed at the liquid–liquid interface  $x = \bar{b}$  follows from the balance of the normal stresses accounting for the surface tension effect. Using the dimensional variables, we present the position of the perturbed interface as

$$r = b + \xi(\theta, z, t), \quad \xi(\theta, z, t) = \delta \exp(\lambda t + in\theta + ikz), \quad (12)$$

where  $\delta$  is an infinitesimally small perturbation amplitude. The capillary pressure  $p_\sigma$  in the linear approximation is given by

$$p_\sigma = \sigma \left[ \frac{1}{b} - \frac{1}{b^2} \left( \xi + \frac{\partial^2 \xi}{\partial \theta^2} \right) - \frac{\partial^2 \xi}{\partial z^2} \right], \quad (13)$$

where  $\sigma$  is the surface tension coefficient. Using (12) and (13) we arrive at the following linearized dimensionless balance of the normal stresses at  $x = \bar{b}$ :

$$\begin{aligned} & \lambda \left[ \rho_{12} \frac{du_2}{dx} - \frac{du_1}{dx} \right] \\ &= \frac{\bar{\delta} k^2}{\bar{a}} (\rho_{12} - 1) V_1^2 + \frac{1}{Re} \left[ \frac{dD}{dx} - 2 \frac{d}{dx} \right] (\eta_{12} u_2 - u_1) \\ & \quad - \rho_{12} \frac{in}{\bar{a}} V_1 \frac{d}{dx} (\rho_{12} u_2 - u_1) - \frac{\bar{\delta} k^2}{We} \left[ \frac{1 - n^2}{\bar{b}^2} - k^2 \right]. \end{aligned} \quad (14)$$

Here  $\bar{\delta} = \delta/d$  and  $We = Gd/\sigma$  is the Weber number. The linearized dimensionless balance of the tangent stresses, which replaces that of (10g) at  $x = \bar{b}$ , reads

$$\frac{d^2 u_1}{dx^2} + k^2 u_1 = \eta_{12} \left[ \frac{d^2 u_2}{dx^2} + k^2 u_2 \right]. \quad (15)$$

To complete the formulation of the boundary conditions at the perturbed interface, we note that the linearized kinematic boundary condition here reads

$$\frac{\partial \xi}{\partial t} = u_i - \frac{V_i}{\bar{b}} \frac{\partial \xi}{\partial \theta}, \quad (16)$$

and yields the following dimensionless kinematic condition at  $x = \bar{b}$ :

$$\lambda \bar{\delta} = u_1 - \frac{in}{\bar{b}} V_1 \bar{\delta}. \quad (17)$$

We have formulated two distinct stability problems. The first deals with the nondeformable interface and is posed by Eqs. (9)–(10). The second accounts for small perturbations of the liquid–liquid interface and is posed by Eqs. (9), (10a), (10b), (10d)–(10f), (11), (14), (15), and (17). We shall refer to them as I and II, respectively.

Note that the requirement  $u_1(\bar{b}) = u_2(\bar{b}) = 0$ , which is equivalent to  $\bar{\delta} = 0$ , reduces problem II to problem I. Note also that problem II should be considered only for  $n > 0$ , since axisymmetric ( $n = 0$ ) deformation of the boundary is incompatible with the mass conservation requirement in the incompressible liquids we are dealing with.

For solution of problems I and II, the marginal Dean number  $De_m$  has to be calculated for each  $n$  and  $k$ , for which the real part of the growth rate  $\lambda$  changes from negative to positive values. Then for given parameters  $\bar{a}$ ,  $\bar{b}$ , and  $We$  the

critical Dean number is defined as  $De_{cr}(\bar{a}, \bar{b}, We) = \min_{n,k} d De_m(\bar{a}, \bar{b}, We, n, k)$ . The values  $n = n_{cr}$  and  $k = k_{cr}$  corresponding to the minimum of  $De_m$ , together with the corresponding eigenfunction of (9), define the most dangerous perturbation. At each marginal point the imaginary part of  $\lambda$  defines the temporal behavior of the marginally unstable perturbation. For  $\text{Im}(\lambda) = 0$  a steady bifurcation (transition from the base state to another steady flow) is expected. For  $\text{Im}(\lambda) \neq 0$  oscillatory instability sets in and the supercritical flow is anticipated to become oscillatory. In the latter case we define  $\omega_m = \text{Im}(\lambda)$  as the marginal frequency of oscillations.

## V. NUMERICAL METHOD

### A. Nondeformable interface

The numerical approach is based on the global Galerkin method with the basis functions satisfying all boundary conditions on the no-slip walls and at the liquid–liquid interface. Zebib<sup>14</sup> and Gelfgat and Tanasawa<sup>9</sup> proposed use of linear superpositions of Chebyshev polynomials to satisfy homogeneous linear boundary conditions for the flow region. This approach is described in detail in Gelfgat<sup>10</sup> and was used for stability analysis of confined flows in rectangular<sup>9,15–17</sup> and cylindrical<sup>18,19</sup> geometries. Now it should be extended so as to include the conditions at the interface in the basis functions defined over the whole flow region.

To formulate the global Galerkin method, we approximate the solution by series defined over the whole interval  $0 \leq x \leq 1$

$$v = \sum_{k=1}^N c_k \varphi_k(x), \quad u = \sum_{k=1}^N d_k \psi_k(x). \quad (18)$$

The basis functions  $\varphi_k(x)$  and  $\psi_k(x)$  comprise different superpositions of Chebyshev polynomials ( $T_n(x) = \cos[n \arccos(x)]$ ) in the subintervals  $0 \leq x \leq \bar{b}$  and  $\bar{b} \leq x \leq 1$ , defined as

$$\begin{aligned} \varphi_k(x) &= \begin{cases} \sum_{l=0}^2 \alpha_{kl}^{(1)} T_{k+l} \left( \frac{x}{\bar{b}} \right), & 0 \leq x \leq \bar{b} \\ \sum_{l=0}^2 \alpha_{kl}^{(2)} T_{k+l} \left( \frac{x - \bar{b}}{1 - \bar{b}} \right), & \bar{b} \leq x \leq 1 \end{cases}, \quad (19) \\ \psi_k(x) &= \begin{cases} \sum_{l=0}^4 \beta_{kl}^{(1)} T_{k+l} \left( \frac{x}{\bar{b}} \right), & 0 \leq x \leq \bar{b} \\ \sum_{l=0}^4 \beta_{kl}^{(2)} T_{k+l} \left( \frac{x - \bar{b}}{1 - \bar{b}} \right), & \bar{b} \leq x \leq 1 \end{cases}. \quad (20) \end{aligned}$$

However, the coefficients  $c_k$  and  $d_k$  remain the same for the whole flow region. The coefficients  $\alpha_{kl}^{(i)}$  are determined after substitution of (19) in the boundary conditions (10a), (10b), (10d) and the coefficients  $\beta_{kl}^{(i)}$  after substitution of (20) in (10a)–(10c) and (10e)–(10g). We use computer algebra to derive analytical expressions for these coefficients (the corresponding expressions can be found at

TABLE I. Convergence of the critical Dean number.

N	Single-fluid case,	Two-fluid case,	Two-fluid case,	Two-fluid case,	Two-fluid case,
	$\bar{b}=0.5,$ $k=3.889, n=0$	nondeformable interface, $\bar{b}=0.5, k=7.2, n=0$	deformable interface, <sup>a</sup> $\bar{b}=0.5, k=7.7, n=1$	deformable interface, <sup>a</sup> $\bar{b}=0.2, k=28.4, n=12$	deformable interface, <sup>a</sup> $\bar{b}=0.9, k=39.0, n=7$
4	37.5349	99.313	99.3258	821.233	358.940
8	37.5287	99.277	99.2845	664.210	350.737
12	37.5287	99.273	99.2811	716.300	351.005
16		99.2735	99.2804	715.067	351.186
20		99.2726	99.2800	712.541	351.306
30		99.2724	99.2800	711.253	351.470
40				710.518	351.549
50				710.147	351.591
60	No change	No change	No change	709.961	351.611
70				709.858	351.614
80				709.813	351.613
90				709.802	351.614
100				709.803	351.614

<sup>a</sup>Result for nondeformable interface differs in the fourth or fifth decimal digit only.

<http://tx.technion.ac.il/~cml/cml/staff/publicat.htm>). Note that the basis functions (19) and (20) satisfy all the boundary conditions (10) analytically.

The inner product is defined as an integral over the whole interval  $0 \leq x \leq 1$  and is calculated as the sum of the integrals in the subintervals  $0 \leq x \leq \bar{b}$  and  $\bar{b} \leq x \leq 1$

$$\langle f, g \rangle = \int_0^1 f(x)g(x)dx = \int_0^{\bar{b}} f(x)g(x)dx + \int_{\bar{b}}^1 f(x)g(x)dx. \tag{21}$$

Therefore, the method remains global, with each of the equations (9) treated separately in the corresponding subinterval. After the Galerkin projections have been applied, Eqs. (9) reduce to the generalized algebraic eigenvalue problem

$$\lambda \mathbf{A} \mathbf{y} = \mathbf{B} \mathbf{y}, \tag{22}$$

where  $\mathbf{A}$  and  $\mathbf{B}$  are matrices and the vector  $\mathbf{y}$  contains all the coefficients  $c_k$  and  $d_k$ . The matrix  $\mathbf{A}$  is nonsingular, such that (22) can be transformed into the classic eigenvalue problem  $\lambda \mathbf{y} = \mathbf{A}^{-1} \mathbf{B} \mathbf{y}$ , which is solved numerically using the QR-decomposition algorithm.

**B. Deformable interface**

To account for the deformable interface, we represent the solution as

$$v = \sum_{k=1}^N c_k \varphi_k(x), \quad u = d_0 \phi(x) + \sum_{k=1}^N d_k \psi_k(x). \tag{23}$$

The bases  $\varphi_k(x)$  and  $\psi_k(x)$  remain unchanged. An additional function  $\phi(x)$  is introduced to satisfy the boundary conditions of stability problem II. The function  $\phi(x)$  is defined as

$$\phi(x) = \begin{cases} \sum_{l=0}^4 \gamma_{Jl}^{(1)} T_{J+l} \left( \frac{x}{\bar{b}} \right), & 0 \leq x \leq \bar{b} \\ \sum_{l=0}^4 \gamma_{Jl}^{(2)} T_{J+l} \left( \frac{x-\bar{b}}{1-\bar{b}} \right), & \bar{b} \leq x \leq 1 \end{cases}, \tag{24}$$

such that the coefficients  $\gamma_{Jl}^{(i)}$  are used to satisfy Eqs. (10a), (10b), (10d), (10e), (11), and (15) subject to the normalization condition  $\phi(\bar{b}) = 1$ . The value of subscript  $J$  is fixed and its choice is arbitrary to within the regularity restriction on matrix  $\mathbf{A}$  in the generalized eigenvalue problem (22) (the coefficients  $\gamma_{Jl}^{(i)}$  also can be found at <http://tx.technion.ac.il/~cml/cml/staff/publicat.htm>).

With the normalization condition  $\phi(\bar{b}) = 1$  applied, the coefficient  $d_0$  manifests itself as the amplitude of the radial velocity at the deformed interface. This coefficient, and the interface amplitude  $\bar{\delta}$ , are defined by the two remaining boundary conditions (14) and (17). Thus, the Galerkin projections of Eqs. (9) together with Eqs. (14) and (17) form a closed algebraic system for calculation of the coefficients  $c_k$  and  $d_k$  ( $k = 1, 2, \dots$ ), as well as of the two additional parameters  $d_0$  and  $\bar{\delta}$ . As mentioned above, the latter manifest themselves as the amplitudes of the normal velocity of the interface and the corresponding perturbation of its position, respectively. The resulting generalized eigenvalue problem is written in the form (22), with the two additional components of the vector  $\mathbf{y}$  equal to  $d_0$  and  $\bar{\delta}$ .

**C. Test calculations**

Table I illustrates the results of the convergence study, which was carried out for the three versions of the Dean problem—the classical, the two-fluid with nondeformable interface and the two-fluid with deformable interface. In all three cases the most dangerous values of  $k$  and  $n$  were taken. Other parameters were  $\bar{a} = 10$ ,  $\rho_{12} = \eta_{12} = 1.1$ , and  $We = 1$ . It is seen that the convergence differs for the lower (i.e.,  $n = 0, 1$ ) and higher ( $n > 5$ ) azimuthal modes. The conver-



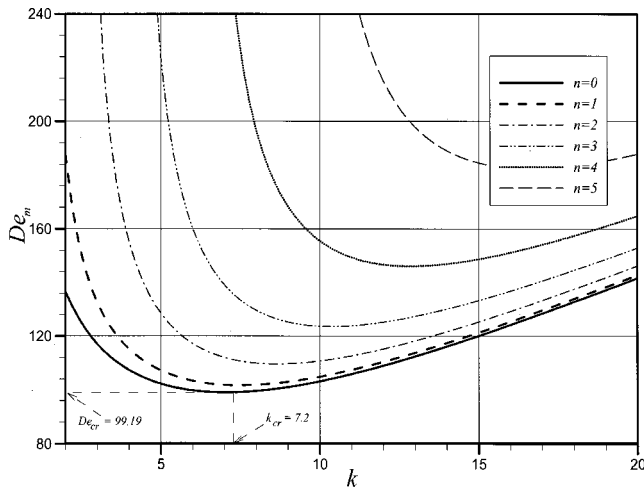


FIG. 2. Stability diagram for  $\rho_{12}=\eta_{12}=1.1$ ,  $\bar{a}=10$ , and  $\bar{b}=0.5$ . Nondeformable interface.

gence of  $De_m$  corresponding to  $n=0, 1$  is rather fast, so that truncation of the series (18) and (23) up to  $N=40-50$  terms yields the convergence up to 5–6 decimal digits. For the higher azimuthal harmonics the convergence is significantly slower, but with  $N=40-50$  terms 3–4 correct digits are still obtainable.

The results described below were obtained with  $N=40$  and some of them were revalidated with  $N=60$ . Note that the critical Dean number for the single-fluid case<sup>2</sup> recalculated according to the present definitions is approximately 37.13, which is in good agreement with the present result, 37.53. Note also that the fast convergence obtained for the single-fluid case is similar to that obtained for the classical Rayleigh–Bénard problem by the same global Galerkin approach.<sup>15</sup>

VI. RESULTS

Stability diagrams were calculated for a fixed inner radius of the channel  $\bar{a}=10$  and fixed viscosity and density ratios  $\rho_{12}=\eta_{12}=1.1$ . Attention was first focused on variation of the stability domain of the flow with the relative depth of the inner layer  $\bar{b}$ . To study how the stability results depend on the fluid properties, the parameters  $\rho_{12}$  and  $\eta_{12}$  were mainly varied between 0.5 and 2. Additional calculations were carried out for  $0.1 \leq \rho_{12} \leq 10$ ,  $0.01 \leq \eta_{12} \leq 10$ , and  $\bar{a}=100$ , but no significant changes in the already obtained results were found.

A. Nondeformable interface, case  $\rho_{12}=\eta_{12}=1.1$

The calculations show that for the nondeformable boundary the axisymmetric mode  $n=0$  remains the most dangerous at  $0.24 < \bar{b} < 0.87$ . A characteristic stability diagram for  $\bar{b}=0.5$  is shown in Fig. 2. It is seen that while the marginal curve  $De_m(k)$  of mode  $n=0$  always remains the lowest, modes  $n=1$  and 2 are very close to it. The minimal values of  $\min_k De_m(k)$  for  $n=0$  and 1 differ only in the fourth decimal digit (see also Table I). This means that even at very small supercriticalities these modes will develop simulta-

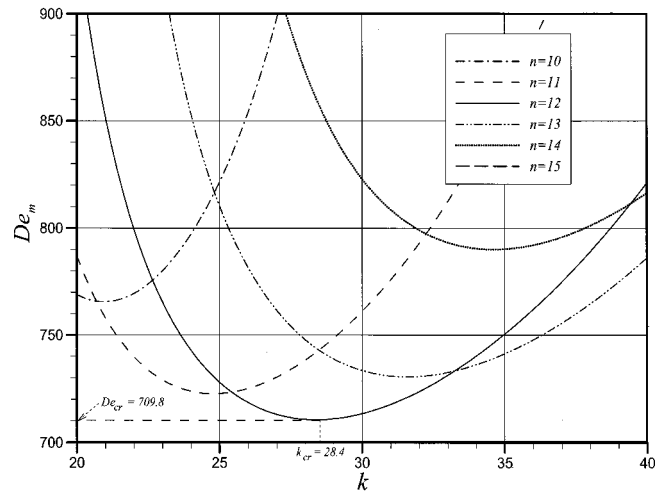


FIG. 3. Stability diagram for  $\rho_{12}=\eta_{12}=1.1$ ,  $\bar{a}=10$ , and  $\bar{b}=0.2$ . Nondeformable interface. Marginal Dean numbers corresponding to the modes  $n < 10$  and  $n > 15$  are above the value  $De=900$ .

neously, which can lead to a three-dimensional flow. Besides this, already at small supercriticalities multiple supercritical flow states (both axisymmetric and three-dimensional) are possible.

As the relative depth of the inner layer increases or decreases from the value  $\bar{b}=0.5$ , the marginal Dean numbers corresponding to the higher azimuthal modes tend to those for  $n=0$  and finally one of these modes becomes the most dangerous. This makes the instability three-dimensional. Figures 3 and 4 illustrate this for  $\bar{b}=0.2$  and  $\bar{b}=0.9$ , respectively. The most dangerous modes being  $n=12$  in the first case and  $n=7$  in the second. Here also several different azimuthal modes have marginal Dean numbers close to the critical, which can lead to multiple three-dimensional supercritical states.

To follow the change of the critical Dean number with variation of the relative depth of the inner layer, the depen-

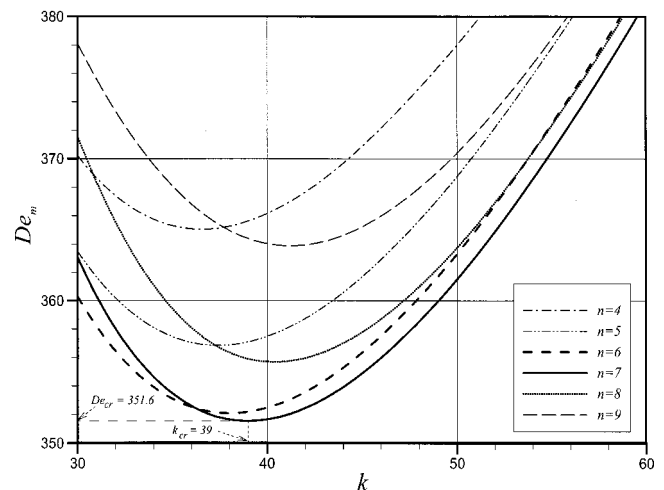


FIG. 4. Stability diagram for  $\rho_{12}=\eta_{12}=1.1$ ,  $\bar{a}=10$ , and  $\bar{b}=0.9$ . Nondeformable interface. Marginal Dean numbers corresponding to the modes  $n < 4$  and  $n > 9$  are above the value  $De=380$ .

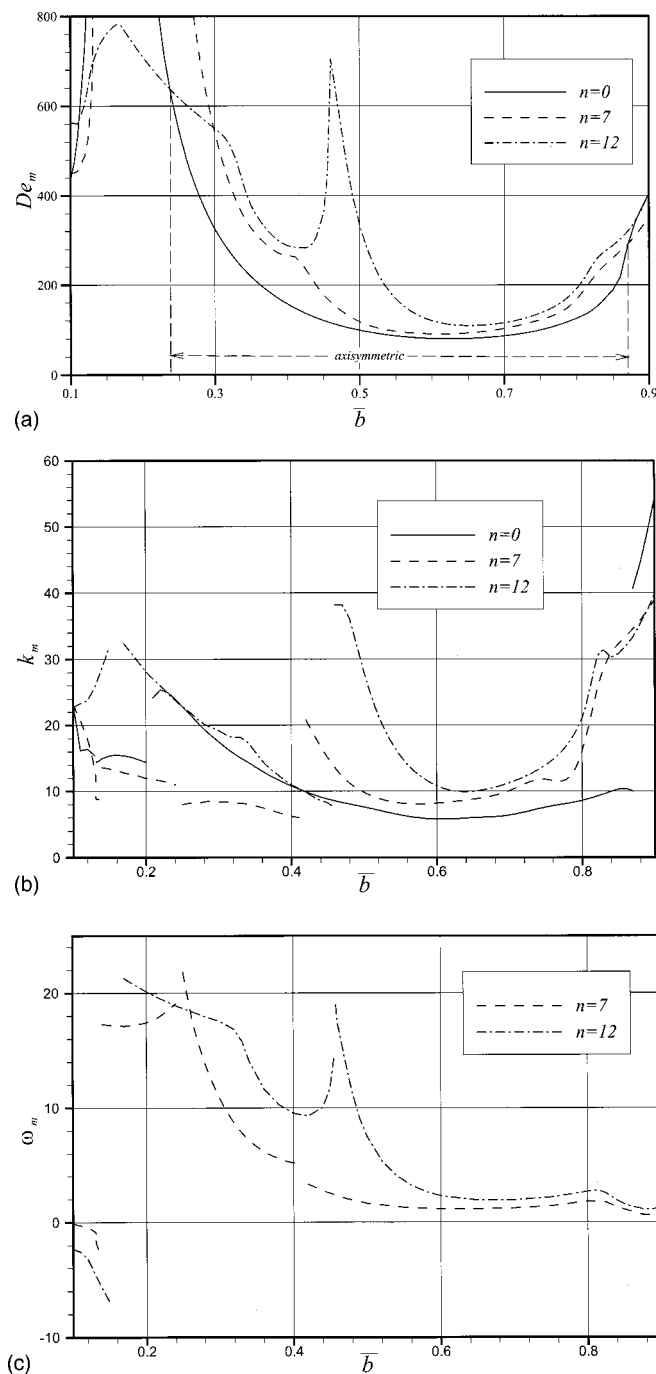


FIG. 5. Change of the marginal values with variation of relative depth of the inner layer,  $\rho_{12} = \eta_{12} = 1.1$ . (a)  $De_m(\bar{b})$ , (b)  $k_m(\bar{b})$ , (c)  $\omega_m(\bar{b})$ .

dences  $De_m(\bar{b})$  for  $n=0, 7$ , and  $12$  are shown in Fig. 5(a). The behavior of the marginal values is nonmonotonic, as a result of switches between perturbation modes [different eigenmodes of the stability problem (9)] corresponding to the same azimuthal wave number  $n$ , as well as to different wave numbers. A switch between perturbation modes is followed by an abrupt change of the marginal axial wave number  $k_m$  and, in the case of the oscillatory instability, an abrupt change of the marginal frequency  $\omega_m$ . The latter is illustrated in Figs. 5(b) and 5(c).

Note that according to the present calculations, the axi-

symmetric instability ( $n=0$ ) is always steady, while three-dimensional instability ( $n>0$ ) is always oscillatory. In the latter case the most dangerous perturbation is proportional to  $\exp[i(\omega_{cr}t + n_{cr}\theta + k_{cr}z)]$ , and therefore, is a spiraling wave which rotates about the axis with the angular velocity  $\omega_{cr}/n_{cr}$  and propagates axially with the traveling velocity  $\omega_{cr}/k_{cr}$ . Note also that the wave rotates codirectionally with the main flow when  $\omega_{cr}>0$ , and in the opposite direction when  $\omega_{cr}<0$ .

Patterns of the spiraling most dangerous three-dimensional perturbations for  $n=7, \bar{b}=0.9$ , and  $n=12, \bar{b}=0.2$  are illustrated in Figs. 6 and 7, respectively. The levels of the isolines are equally distanced between the maximal and minimal perturbation values. As noted, the perturbation is defined to within multiplication by a constant. For better representation of the three-dimensional functions, the radial coordinate inside the annulus is zoomed by a factor of 20. The axial coordinate is varied between zero and  $2\pi/k_{cr}$ .

**B. Nondeformable interface: Effect of the variation of  $\rho_{12}$  and  $\eta_{12}$**

Decrease of the viscosity ratio  $\eta_{12}$  leads to the stabilization of all three-dimensional modes. As a result, the primary axisymmetric instability is restored. Thus, at  $\rho_{12}=1.1, \bar{a}=10$ , and  $\bar{b}=0.9$  the axisymmetric steady perturbation is dominant for  $\eta_{12}<0.86$ . This is illustrated in Fig. 8 where the dependencies  $De_m(k, n)$  are shown for  $\eta_{12}=0.8$  and  $\eta_{12}=0.9$ . Note that the marginal Dean numbers corresponding to higher azimuthal modes ( $n \leq 6$ ) are almost the same for  $\eta_{12}=0.8$  and  $0.9$ , while those of the lower modes increase significantly when the viscosity ratio  $\eta_{12}$  changes from  $0.8$  to  $0.9$ . As a result, the lowest critical Dean number of Fig. 8(a) corresponds to the axisymmetric perturbation with  $n_{cr}=0$  (which means that the instability sets in due to it), whereas that of Fig. 8(b)—to the nonaxisymmetric one with  $n_{cr}=6$ .

The stability analysis for the single-layer case assuming the stress-free boundary conditions at the outer boundary of the layer yields the following result: The instability is axisymmetric ( $n_{cr}=0$ ), with  $De_{cr}=23.23, k_{cr}=2.07$ , and  $\omega_{cr}=0$ . This indicates a possible similarity between the instability in a single-layer case with a stress-free outer boundary and a two-layer case with a less viscous outer fluid layer. However, the present formulation is not well-suited for the study of the limiting case  $\eta_{12} \rightarrow 0$ , because the basic flow in the outer layer (6b) tends to infinity under these conditions. Besides this, too many basis functions (19) and (20) are needed to describe the discontinuity of the derivatives in the boundary conditions (10f) and (10g). To study a possible similarity it is necessary to compare the perturbation patterns for the single-layer and two-layer cases. Figure 9 shows the perturbation  $u(x)$  for these cases. Calculations for the two-layer case were done for  $\bar{b}=0.9, \rho_{12}=1.1$ , and the viscosity ratios  $\eta_{12}=0.1$  and  $0.01$ . Note that the perturbation is a real function in the case  $\omega_{cr}=0$ . The perturbation patterns in the single layer and in the inner layer ( $0 < x < 0.9$ ) are different at  $\eta_{12}=0.1$  and show some similarity at  $\eta_{12}=0.01$ . However, the maximal value of the perturbation in the outer layer

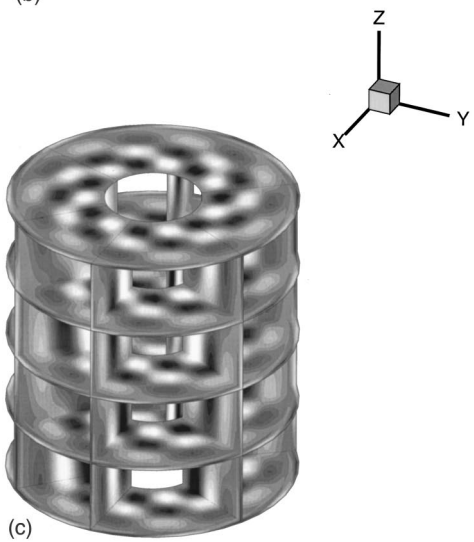
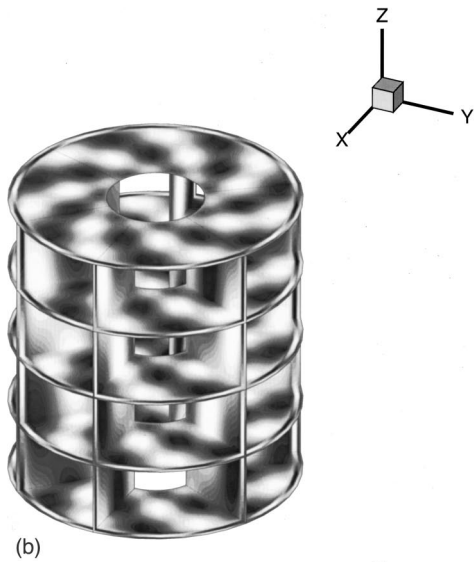
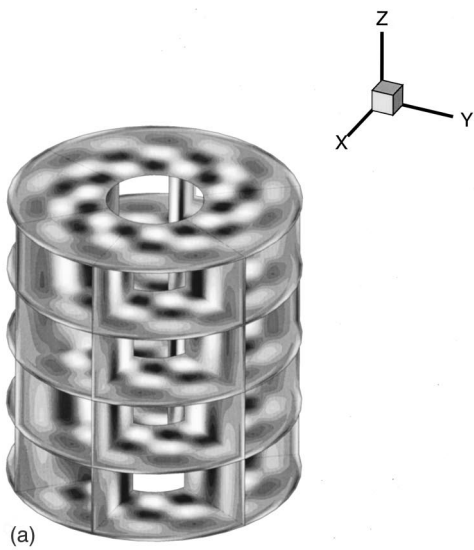


FIG. 6. Perturbation of the velocity components for  $\bar{b}=0.9$ ,  $De_{cr}=351.5$ ,  $n_{cr}=7$ ,  $k_{cr}=39$ ,  $\omega_{cr}=0.576$ . The radial coordinate in the interval  $\bar{a} \leq r \leq \bar{a} + \bar{b}$  is zoomed by the factor of 20. The axial coordinate varies in the interval  $0 \leq z \leq 2\pi/k_{cr}$ . (a) Perturbation of the radial velocity, (b) perturbation of the azimuthal velocity, (c) perturbation of the axial velocity.

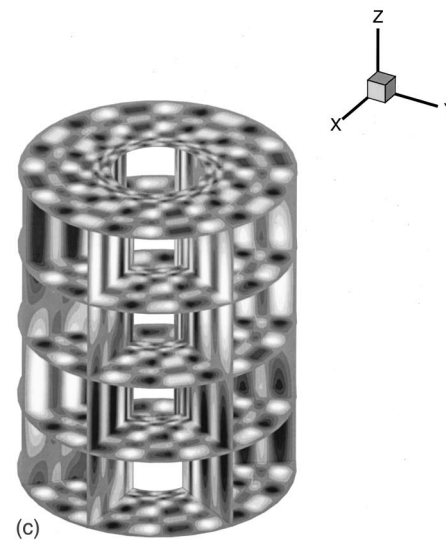
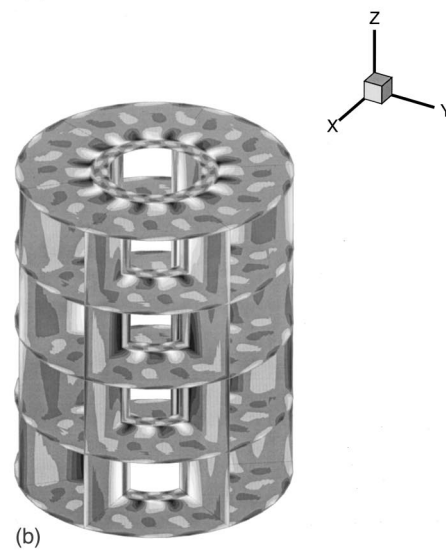
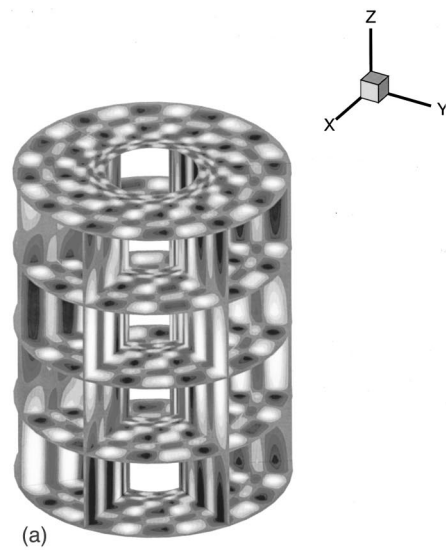


FIG. 7. As Fig. 6 for  $\bar{b}=0.2$ ,  $De_{cr}=710.5$ ,  $n_{cr}=12$ ,  $k_{cr}=28.2$ ,  $\omega_{cr}=1.31$ .

( $0.9 < x < 1$ ) grows with the decrease of  $\eta_{12}$ . At  $\eta_{12}=0.01$  the maximal values of the perturbation in the inner and outer layers become almost equal (cf. Fig. 9). Therefore, it cannot be concluded that the onset of the instability takes place in



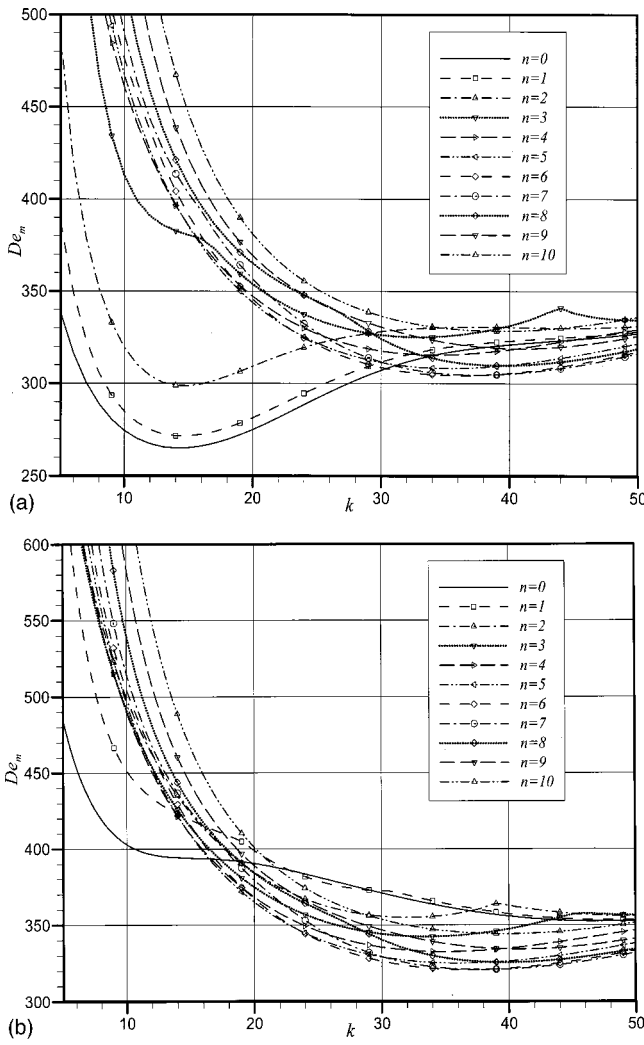


FIG. 8. Stability diagram for  $\rho_{12}=1.1$ ,  $\bar{a}=10$ , and  $\bar{b}=0.9$ . Nondeformable interface. (a)  $\eta_{12}=0.8$ , (b)  $\eta_{12}=0.9$ .

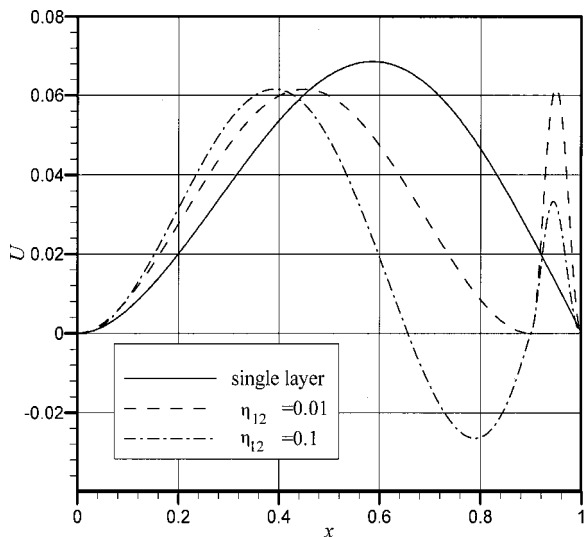


FIG. 9. Comparison of the perturbation  $u(x)$  for the single layer and two-layer cases with a small viscosity ratio.

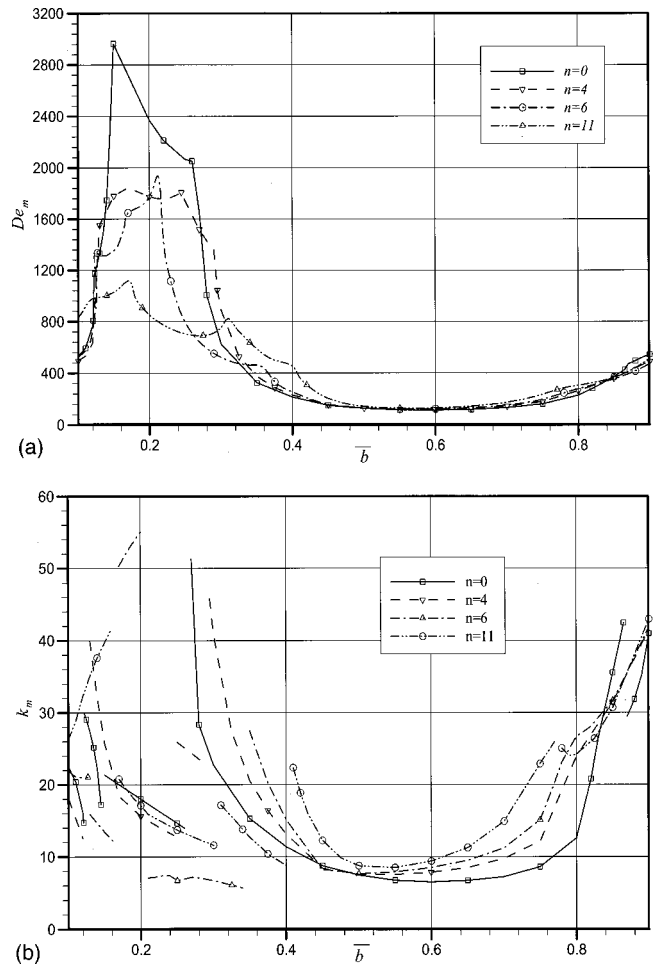


FIG. 10. Change of the marginal values with variation of relative depth of the inner layer,  $\rho_{12}=1.1$ ,  $\eta_{12}=2$ . (a)  $De_m(\bar{b})$ , (b)  $k_m(\bar{b})$ .

the inner layer only. Besides this, the critical azimuthal wavelengths are  $k_{cr}=10.5$  and  $k_{cr}=6.3$  for  $\eta_{12}=0.1$  and  $0.01$ , respectively, which is distinct from  $k_{cr}=2.07$  for the single-layer case. It can be concluded that even when viscosity of the outer layer is much smaller than that of the inner one, the onset of the instability takes place in both layers simultaneously, so that there is no direct similarity with the single-layer case.

Increase of the viscosity ratio makes for more three-dimensional modes to become dominant. This is illustrated in Fig. 10 for  $\eta_{12}=2$ . In this case three three-dimensional modes  $n=4, 6$ , and  $11$  (instead of two modes  $n=7$  and  $12$  at  $\eta_{12}=1.1$ , Fig. 5) together with the axisymmetric one ( $n=0$ ) replace each as  $\bar{b}$  varies. Note also that the switch from the axisymmetric to three-dimensional instability takes place at  $\bar{b}<0.325$  and  $\bar{b}>0.84$ , so that the range of the values of  $\bar{b}$  corresponding to the axisymmetric instability is smaller than that for  $\eta_{12}=1.1$  ( $0.24<\bar{b}<0.87$ ).

Dependence of the marginal Dean numbers and the marginal axial wavelength on the density ratio  $\rho_{12}$  is shown in Fig. 11 for  $\eta_{12}=1.1$  and the three cases having different critical azimuthal wave numbers in Fig. 5. The common tendency for small  $\rho_{12}$  is an increase of the marginal Dean num-

bers as the density ratio decreases. At large values of  $\rho_{12}$  the marginal parameters ( $De_m$  and  $k_m$ ) slowly decrease with the growth of the density ratio, tending to certain limit values as  $\rho_{12} \rightarrow \infty$ . At moderate values of  $\rho_{12}$  the dependences can be monotonic (as for  $\bar{b}=0.5, n=0$  and  $\bar{b}=0.9, n=7$ ) or non-monotonic (as for  $\bar{b}=0.2, n=12$ ). Note that the three modes shown in Fig. 11 do not remain critical for the whole range of  $\rho_{12}$  considered. One can conclude that the critical parameters are strongly dependent on the fluids properties, as well as on the geometric parameters, so that each particular case should be considered separately.

### C. Deformable interface

To estimate the Weber number, we note that  $We = Gd/\sigma = Re^2 \eta_1^2 / (d\sigma\rho_1)$ . Following experiments,<sup>7</sup> we estimate  $\eta_1 \sim 7.5 \times 10^{-3} \text{ kg/m}\cdot\text{s}$ ,  $\rho_1 \sim 1500 \text{ kg/m}^3$ ,  $d \sim 10^{-2} \text{ m}$ , and  $\sigma \sim 5 \times 10^{-2} \text{ kg/s}^2$ . This yields  $We \sim 10^{-4} Re^2$ . According to the results obtained for the nondeformable interface, the critical Reynolds number is of order  $10^2 - 10^3$ , hence the estimate of the Weber number is  $We \sim 1 - 10^2$ . However, the calculations show that accounting for a deformable surface has a negligible effect on the instability of the flow considered. We tried to generate unstable modes, which are strongly affected by the interface deformation, by introducing a vanishing surface tension, and increased the Weber number up to  $We = 10^6$ . We also varied the density and viscosity ratios between 0.1 and 10 and made calculations for  $\bar{a} = 100$ . Still, in all calculations the critical Dean numbers corresponding to the cases of a deformable and a nondeformable interface differed only in the fourth or fifth decimal digit. For high azimuthal modes ( $n > 10$ ) this difference appeared sometimes in the third digit. It was concluded that the instability is related to the appearance of the Dean vortices, and is virtually unaffected by deformation of the liquid-liquid interface. The smallness of the effect of the latter may be due to the fact that the considered model accounts only for a large inner radius of the annulus  $\bar{a}$ , making the initial curvature of the interface negligibly small. Note also that the effect of gravity is neglected. However, the deformation should be accounted for in supercritical regimes, as was done for the two-layer Couette flow in Ref. 13.

## VII. CONCLUSION

An extension of the global Galerkin approach to stability analysis of flows in a two-fluid system is presented. The proposed numerical technique allows one to implement all the boundary conditions (including those imposed on the liquid-liquid interface) into Galerkin basis functions. This reduces the hydrodynamic stability problem to a generalized algebraic eigenvalue problem without additional algebraic constraints. A special numerical treatment of small deformations of the liquid-liquid interface, including capillary effects, is proposed.

The numerical approach developed was applied to the two-fluid Dean problem. The onset of the instability, which manifests itself in appearance of axisymmetric or three-dimensional vortices, was studied for different widths of the

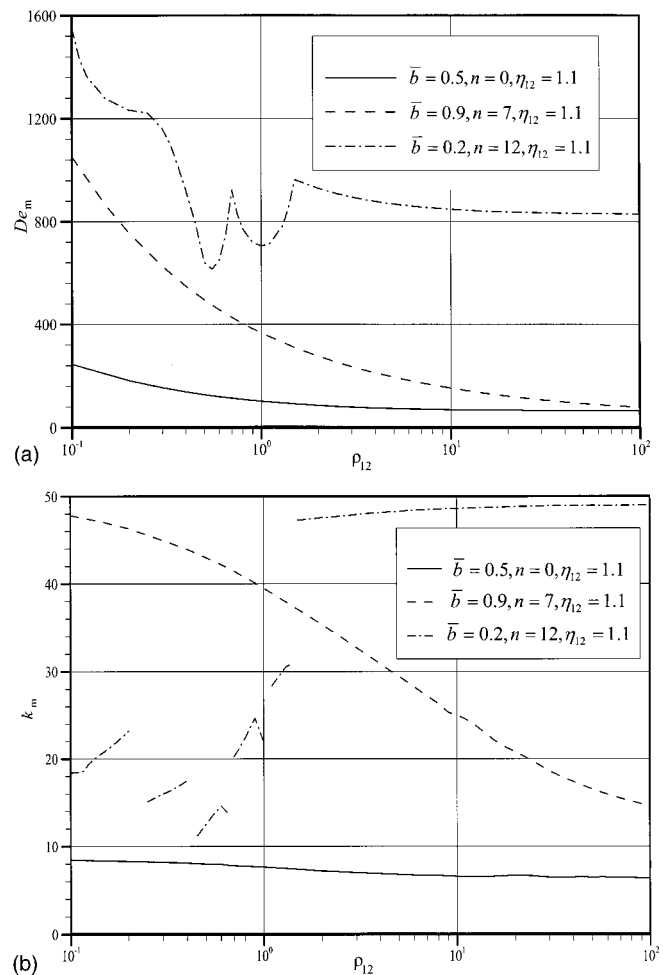


FIG. 11. Change of the marginal values with variation of the density ratio. (a)  $De_m(\rho_{12})$ . (b)  $k_m(\rho_{12})$ .

fluid layers. For a fixed inner radius of the annulus ( $\bar{a} = 10$ ) and fixed viscosity and density ratios ( $\rho_{12} = \eta_{12} = 1.1$ ) it was shown that the instability is axisymmetric when the relative depth of the inner layer lies in the range  $0.24 < \bar{b} < 0.97$ , and three-dimensional otherwise. At the same time, onset of the instability (axisymmetric, as well as three-dimensional) is also characterized by development of several three-dimensional modes, which become unstable already at very small supercriticalities. Therefore, the resulting supercritical state should be expected to be three-dimensional. Moreover, multiplicity of stable supercritical states seems to be possible.

Variation of the viscosity and density ratios  $\rho_{12}$  and  $\eta_{12}$  do not change the above qualitative conclusions. However, the dependence of the critical Dean number and critical axial wavenumber on other governing parameters (fluids properties and geometry of the system) is found to be strong. Similarly to the previously studied stability problems,<sup>15-19</sup> the critical parameters must be calculated for each particular case separately. Note also that the physics of the instability found for the two-layer systems is the same as in the classical Dean problem. The instability is caused by the disbalance between the centrifugal and viscous forces. However, in the two-layer case the instability is affected by the interaction of

the perturbations located in each layer, which changes the critical wave numbers and can lead to three-dimensional instabilities.

## ACKNOWLEDGMENTS

This research was supported by BSF (US–Israel Binational Science Foundation) Grant No. 97-118 and by the Center for Absorption in Science, Israel Ministry of Immigrant Absorption (to A.G.).

- <sup>1</sup>W. R. Dean, "Fluid flow in a curved channel," *Proc. R. Soc. London, Ser. A* **121**, 402 (1928).
- <sup>2</sup>W. H. Reid, "On the stability of viscous flow in a curved channel," *Proc. R. Soc. London, Ser. A* **244**, 186 (1958).
- <sup>3</sup>R. D. Gibson and A. E. Cook, "The stability of curved channel flow," *Q. J. Mech. Appl. Math.* **27**, 149 (1974).
- <sup>4</sup>S. A. Berger, L. Talbot, and L. S. Yao, "Flow in curved pipes," *Annu. Rev. Fluid Mech.* **15**, 461 (1983).
- <sup>5</sup>A. Nakayama, N. Kokubo, T. Ishida, and F. Kuwahara, "Conjugate numerical model for cooling a fluid flowing through a spiral coil immersed in a chilled water container," *Numer. Heat Transfer, Part A* **37**, 155 (2000).
- <sup>6</sup>T. Kluge, C. Rezende, D. Wood, and G. Belfort, "Protein transmission during Dean vortex microfiltration of yeast suspensions," *Biotechnol. Bioeng.* **65**, 649 (1999).
- <sup>7</sup>G. Baier and M. D. Graham, "Two-fluid Taylor–Couette flow experiments and linear theory for immiscible liquids between corotating cylinders," *Phys. Fluids* **10**, 3045 (1998).
- <sup>8</sup>G. Baier, T. M. Grateful, M. D. Graham, and E. N. Lightfoot, "Prediction of mass transfer rates in spatially periodic flows," *Chem. Eng. Sci.* **54**, 343 (1999).
- <sup>9</sup>A. Yu. Gelfgat and I. Tanasawa, "Numerical analysis of oscillatory instability of buoyancy convection with the Galerkin spectral method," *Numer. Heat Transfer, Part A* **25**, 627 (1994).
- <sup>10</sup>A. Yu. Gelfgat, "Two- and three-dimensional instabilities of confined flows: Numerical study by a global Galerkin method," *Computational Fluid Dynamics J.* **9**, 437 (2001).
- <sup>11</sup>D. D. Joseph and Y. Y. Renardy, *Fundamentals of Two-Fluid Dynamics. Part I: Mathematical Theory and Applications*, (Springer-Verlag, Berlin 1993).
- <sup>12</sup>K. Fujimura and Y. Y. Renardy, "The 2:1 steady/Hopf mode interaction in the two-layer Bénard problem," *Physica D* **85**, 25 (1995).
- <sup>13</sup>J. Li, Y. Renardy, and M. Renardy, "A numerical study of periodic disturbances on two-layer Couette flow," *Phys. Fluids* **10**, 3056 (1998).
- <sup>14</sup>A. Zebib, "A Chebyshev method for the solution of boundary value problems," *J. Comput. Phys.* **53**, 443 (1984).
- <sup>15</sup>A. Yu. Gelfgat, "Different modes of Rayleigh–Bénard instability in two- and three-dimensional rectangular enclosures," *J. Comput. Phys.* **156**, 300 (1999).
- <sup>16</sup>A. Yu. Gelfgat, P. Z. Bar-Yoseph, and A. L. Yarin, "On oscillatory instability of convective flows at low Prandtl number," *J. Fluids Eng.* **119**, 823 (1997).
- <sup>17</sup>A. Yu. Gelfgat, P. Z. Bar-Yoseph, and A. L. Yarin, "Stability of multiple steady states of convection in laterally heated cavities," *J. Fluid Mech.* **388**, 315 (1999).
- <sup>18</sup>A. Yu. Gelfgat, P. Z. Bar-Yoseph, and A. Solan, "Vortex breakdown and instability of swirling flow in a cylinder with rotating top and bottom," *Phys. Fluids* **8**, 2614 (1996).
- <sup>19</sup>A. Yu. Gelfgat, P. Z. Bar-Yoseph, and A. Solan, "Stability of confined swirling flow with and without vortex breakdown," *J. Fluid Mech.* **311**, 1 (1996).